

## *Nonlinear regional warming with increasing CO<sub>2</sub> concentration*

Article

Good, P., Lowe, J. A., Andrews, T., Wiltshire, A., Chadwick, R., Ridley, J. K., Menary, M. B., Bouttes, N., Dufresne, J.-L., Gregory, J. M. ORCID: <https://orcid.org/0000-0003-1296-8644>, Schaller, N. and Shiogama, H. (2015) Nonlinear regional warming with increasing CO<sub>2</sub> concentration. *Nature Climate Change*, 5 (2). pp. 138-142. ISSN 1758-678X doi: 10.1038/nclimate2498 Available at <https://centaur.reading.ac.uk/39127/>

It is advisable to refer to the publisher's version if you intend to cite from the work. See [Guidance on citing](#).

To link to this article DOI: <http://dx.doi.org/10.1038/nclimate2498>

Publisher: Nature Publishing Group

All outputs in CentAUR are protected by Intellectual Property Rights law, including copyright law. Copyright and IPR is retained by the creators or other copyright holders. Terms and conditions for use of this material are defined in the [End User Agreement](#).

[www.reading.ac.uk/centaur](http://www.reading.ac.uk/centaur)

**CentAUR**

Central Archive at the University of Reading

Reading's research outputs online

# **Nonlinear regional warming at higher CO<sub>2</sub> concentrations**

**Peter Good<sup>1</sup>, Jason A. Lowe<sup>1</sup>, Timothy Andrews<sup>1</sup>, Andrew Wiltshire<sup>1</sup>, Robin  
Chadwick<sup>1</sup>, Jeff K Ridley<sup>1</sup>, Matthew B Menary<sup>1</sup>, Nathaëlle Bouttes<sup>2</sup>, Jean Louis  
Dufresne<sup>3</sup>, Jonathan M Gregory<sup>2,1</sup>, Nathalie Schaller<sup>4,5</sup>, Hideo Shiogama<sup>6</sup>**

<sup>1</sup> Met Office Hadley Centre, Exeter, United Kingdom

<sup>2</sup> NCAS-Climate, University of Reading, Reading, United Kingdom

<sup>3</sup> Laboratoire de Météorologie Dynamique, Institut Pierre Simon Laplace,  
Paris, France

<sup>4</sup> Institute for Atmospheric and Climate Science, Department of Environmental Sciences,  
Swiss Federal Institute of Technology, Zurich, Switzerland

<sup>5</sup> Atmospheric, Oceanic and Planetary Physics, University of Oxford, Parks Road, Oxford  
OX1 3PU, United Kingdom

<sup>6</sup> Climate Risk Assessment Section, Centre for Global Environmental Research,  
National Institute for Environmental Studies, Tsukuba, Japan

*To be submitted to Nature Climate Change*

Contact information (corresponding author with asterisk)

peter.good@metoffice.gov.uk\*

23    jason.lowe@metoffice.gov.uk  
24    timothy.andrews@metoffice.gov.uk  
25    andy.wiltshire@metoffice.gov.uk  
26    robin.chadwick@metoffice.gov.uk  
27    jeff.ridley@metoffice.gov.uk  
28    matthew.menary@metoffice.gov.uk  
29    n.bouttes@reading.ac.uk  
30    Jean-Louis.Dufresne@lmd.jussieu.fr  
31    j.m.gregory@reading.ac.uk  
32    Schaller@atm.ox.ac.uk  
33    shiogama.hideo@nies.go.jp  
34  
35  
36  
37  
38

In the debate on acceptable levels of climate change, and for planning adaptation measures, stakeholders need regional-scale climate projections including the range of plausible warming rates. To assess the benefits of mitigation, it is important to understand whether some locations may see disproportionately high or low warming from additional forcing above targets such as 2 K<sup>1</sup>. There is an urgent need to narrow uncertainty<sup>2</sup> in this nonlinear warming, which requires understanding how climate changes as forcings increase from medium to high levels. However, quantifying and understanding regional nonlinear processes is challenging. Here we show that regional-scale warming can be strongly super-linear to successive CO<sub>2</sub> doublings, using five different climate models. Ensemble-mean warming is super-linear over most land locations. Further, the inter-model spread tends to be amplified at higher forcing levels, as nonlinearities grow – especially when considering changes per K of global warming. Regional nonlinearities in surface warming arise from nonlinearities in global-mean radiative balance, the Atlantic Meridional Overturning Circulation, surface snow/ice cover and evapotranspiration. In quantifying and understanding the benefits of mitigation, potentially-avoidable climate change (the difference between business-as-usual and mitigation scenarios) and unavoidable climate change (change under strong mitigation scenarios) may need different treatments.

Linear assumptions affect stakeholder advice in various ways<sup>1,3-7</sup>. Fast simplified models<sup>1,5,7</sup> (especially integrated assessment models), for quantifying climate change under many policy scenarios, often assume climate change is the same for each CO<sub>2</sub> doubling. Some studies make a less strong assumption: that regional climate is linear in global warming<sup>3,4,6</sup>. Also, studies of physical mechanisms often explore just one time period of one forcing scenario. An implied linear assumption here is that the

physical mechanisms are similar under other scenarios or for other time periods (not necessarily true in a nonlinear system).

To quantify nonlinearities, the linear response must first be carefully defined. Even in a linear system the spatial patterns of climate change (per CO<sub>2</sub> doubling or per K of global warming) can be different in different forcing scenarios or evolve during a given scenario. This is because of different timescales of response within a system<sup>8-10</sup>. For example, warming over the Southern Ocean lags the global mean<sup>10</sup>. Therefore, the spatial pattern of warming just after a CO<sub>2</sub> change is different than that several decades later.

Our experimental design is chosen to separate linear and nonlinear mechanisms. We use abruptCO<sub>2</sub> experiments, initialized from a pre-industrial control experiment. The CO<sub>2</sub> concentration is changed abruptly, then held constant for 150 years, revealing the model response over different timescales. The abrupt4xCO<sub>2</sub> experiment (with CO<sub>2</sub> quadrupled from pre-industrial levels) has similar forcing magnitude as a business-as-usual scenario by 2100<sup>11</sup>. The abrupt2xCO<sub>2</sub> experiment is identical to abrupt4xCO<sub>2</sub> but with half the CO<sub>2</sub> concentration (with forcing between that reached under RCP2.6 and RCP4.5 scenarios by year 2100<sup>11</sup>). A transient forcing experiment ('1pctCO<sub>2</sub>'), where CO<sub>2</sub> is increased by 1% per year, is also used. We start with results from the HadGEM2-ES climate model.

The abruptCO<sub>2</sub> experiments are highly idealised. Therefore, we first show that their behaviour is comparable to the more policy-relevant 1pctCO<sub>2</sub> experiment, and detect nonlinearities in the 1pctCO<sub>2</sub> response. It is possible to use a simple linear

combination of abruptCO<sub>2</sub> responses to estimate climate change under a transient forcing experiment<sup>12,13</sup>. This linear method performs well when the end of the 1pctCO<sub>2</sub> experiment (near 4xCO<sub>2</sub>) is reconstructed from the abrupt4xCO<sub>2</sub> response (Figure 1b). This shows that the abrupt4xCO<sub>2</sub> experiment features realistic physical mechanisms. It does not mean that temperature responses are linear (conceptually, it is like a local linear approximation to a curve). The importance of nonlinearity is revealed in the relatively poor performance when the abrupt2xCO<sub>2</sub> response is used instead (Figure 1a); while for the middle of 1pctCO<sub>2</sub> (near 2xCO<sub>2</sub>), the reconstruction using abrupt4xCO<sub>2</sub> is much worse than that using abrupt2xCO<sub>2</sub> (compare Figures 1c,d). The linear method is only accurate for periods in the transient experiment with forcing matching that of the abruptCO<sub>2</sub> experiment: climate patterns are therefore different for different CO<sub>2</sub> concentrations – which is evidence of nonlinearity.

Having detected nonlinearities in the 1pctCO<sub>2</sub> experiment, we characterise them more clearly by analysing the abruptCO<sub>2</sub> experiments directly. This experimental design has two significant advantages over the 1pctCO<sub>2</sub> scenario. First, temperature responses in the two abruptCO<sub>2</sub> experiments may be compared at the same timescale after CO<sub>2</sub> is changed (eliminating complications due to linear effects from different timescales of response). Secondly, noise from internal variability may be reduced through long-term means. Assuming that the balance of mechanisms should be stable after the initial ocean mixed-layer warming, we average over years 50-149 of each experiment (Supplementary Figure 1). For abrupt2xCO<sub>2</sub>, these 100-year means correspond roughly to the results for year 2100 of a CO<sub>2</sub>-only version of rcp4.5 (and about double this for abrupt4xCO<sub>2</sub>).

We compare temperature responses to a first and second CO<sub>2</sub> doubling. Current linear methods that parameterise forcing (most integrated assessment and energy balance models) assume that radiative forcing is exactly linear in log(CO<sub>2</sub>) – and equivalently, that each CO<sub>2</sub> doubling produces the same forcing change<sup>1,5</sup>. In HadGEM2-ES, the two doublings give very similar forcing changes<sup>14</sup>. The response to the first doubling is given by abrupt2xCO<sub>2</sub> minus the pre-industrial control; that for the second doubling by abrupt4xCO<sub>2</sub> minus abrupt2xCO<sub>2</sub> (both are averaged over years 50-149). We quantify nonlinearities by the 'doubling difference': the response to the second doubling minus that for the first (Figure 2a); and the 'doubling ratio': the second doubling divided by the first (Figure 2b). Current linear models would have zero doubling difference everywhere.

The doubling ratio in global-mean warming is 1.18 (the second CO<sub>2</sub> doubling produces more warming than the first). Global-scale nonlinearity has been attributed, in other models, to changes in water-vapor and cloud feedbacks, opposed by changes in albedo and lapse-rate feedbacks<sup>15-17</sup>. In some climate models, variation in forcing per CO<sub>2</sub> doubling would also affect the global doubling ratio<sup>15-17</sup>. Regional variation in doubling ratio is broad, however: 5% of the land surface has a doubling ratio outside the range 0.9-1.65 (Supplementary Figure 5a). Gradients of the doubling ratio across continents are strong (Figure 2b), notably over the Americas and Europe, pointing to important regional mechanisms.

We scale out global-mean nonlinearity (Methods) and then focus on the remaining features (see Figure 2c) one by one. The positive area in the north Atlantic, near Greenland, appears to be associated with a nonlinear response of the Atlantic



Meridional Overturning Circulation (AMOC)<sup>18</sup>. In HadGEM2-ES, the maximum Atlantic overturning near 30N weakens about 35% less under a second CO<sub>2</sub> doubling than under the first (a positive doubling difference). We can estimate the effect on surface temperature by scaling the regional temperature response in a separate freshwater hosing experiment (where freshwater is added to the high-latitude north Atlantic to induce AMOC weakening). We multiplied this temperature response pattern by the ratio: (doubling difference for AMOC index) / (AMOC index response in the hosing experiment). The resulting pattern (Figure 2d) features a north Atlantic anomaly similar to that in Figure 2c. This suggests that the north Atlantic nonlinearity is indeed driven by the nonlinear AMOC response. AMOC nonlinearity may arise from variation in the salt-advection feedback (which affects the AMOC strength)<sup>19</sup>. The AMOC transports heat to the North Atlantic, so a positive doubling difference in the AMOC causes positive doubling differences in North Atlantic surface temperatures.

To reveal other nonlinear mechanisms, we subtract the AMOC pattern (Figure 2d) from that in Figure 2c. The residual (Figure 2e) is associated with mechanisms other than those in the global mean energy balance or the AMOC. The North Atlantic positive feature has been effectively removed.

The remaining high-latitude temperature nonlinearities are largely driven by a nonlinear albedo feedback<sup>18,20</sup> (which is dominated by changes in ice and snow cover). It is nonlinear<sup>21</sup> as it becomes zero when ice/snow is either absent or so thick that its extent changes little under warming. The patterns in the doubling difference of sea ice fraction (Figure 2f) match closely the high latitude patterns of temperature doubling

difference (Figure 2e), with sea-ice albedo feedbacks driving temperature nonlinearity (supplementary material).

The final mechanism we study involves land evapotranspiration. Soil moisture-temperature feedbacks can be nonlinear<sup>22</sup>: feedback is small when soil moisture is saturated, or so low that moisture is tightly bound to the soil (in both regimes, evaporation is insensitive to change in soil moisture)<sup>23</sup>. Nonlinear behaviour could also occur through the response of plant stomata (and hence transpiration) to increased CO<sub>2</sub><sup>24</sup>, or through nonlinear precipitation change<sup>25,26</sup>. To investigate this type of effect, we calculate the ratio of mean surface sensible heat and mean surface latent heat fluxes (the Bowen ratio) in the two abruptCO<sub>2</sub> experiments. Much of the temperature nonlinearity over mid/low latitude land (Figure 2g) is associated with change in the Bowen ratio (see Figure 2h). Regions where the Bowen ratio is substantially larger at 4xCO<sub>2</sub> than at 2xCO<sub>2</sub> (red in Figure 2h) have more restricted evaporation: more incident heat is lost as sensible heat, causing further warming. This does not occur where the Bowen ratio is already larger than 1 at 2xCO<sub>2</sub> (e.g. the Sahara, where most turbulent heat is sensible even at 2xCO<sub>2</sub>). These regions are masked in Figure 2h. The most strongly superlinear warming occurs over the Amazon in this model (doubling ratios of 80% are driven by the response of forest tree stomata to CO<sub>2</sub>, with a longer-term response from reduced vegetation productivity - supplementary material; these mechanisms are highly uncertain).

Further to our analysis of HadGEM2-ES we find that nonlinearity is similarly important in four other climate models: NCAR-CESM1, IPSL CM5A-LR, MIROC5 T42 and HadCM3. These models show doubling ratios over land comparable to those

in HadGEM2-ES (supplementary Figure 5a). Over most land locations, the ensemble mean doubling difference is comparable to the ensemble standard deviation for warming from the first doubling (supplementary Figure 5b). That is, the range of warmings simulated by this ensemble is quite different for the first and second CO<sub>2</sub> doublings. The models do show differences in spatial patterns of nonlinear warming. Consequently, the ensemble mean pattern (Figure 3) is smoother than that of any individual model. However, some continental-scale patterns across Europe, North and South America and tropical Africa are similar between Figures 2b and 3.

Nonlinearity has implications not just for the ensemble mean, but also for the spread of model projections. In general, an increased spread at higher forcing should be expected: the relative importance of nonlinear mechanisms grows with increasing forcing, so their contribution to model spread does likewise. Conceptually, this is like including an extra uncertain process at higher CO<sub>2</sub> concentrations. This inflation in model spread at higher forcing is large when nonlinearities are uncertain (supplementary material), and appears to be especially relevant for change per K of global warming. We calculated the ensemble standard deviation in regional warming per K of global warming. Over 30% of land, the ensemble spread is at least 40% larger for the second doubling than for the first doubling (not driven by internal variability – Supplementary Material). This corresponds to a doubling of variance - driven by uncertain nonlinear mechanisms. This finding is important for work quantifying and reducing model uncertainty. It implies that the additional regional warming under a business-as-usual scenario (over and above that in a mitigation scenario) may be more uncertain than the warming under a mitigation scenario - a fact missed by previous linear impacts assessments<sup>1,3,4</sup>. Secondly, different techniques

may be needed to reduce model uncertainty in these two aspects of climate change: uncertainty from nonlinear mechanisms being relatively more important at higher than at lower forcing levels.

The mechanisms of nonlinear warming identified in HadGEM2-ES also operate in the other four models studied. All have a positive global-mean temperature nonlinearity (Supplementary Table 1). As done for HadGEM2-ES, we scale this global-mean nonlinearity out and discuss regional patterns. Most of the remaining temperature nonlinearities over North-West Europe are associated with the AMOC: the magnitude of this nonlinearity is predicted simply by scaling the HadGEM2-ES hosing experiment by the AMOC doubling difference from each model (Figure 4a). While there is significant model spread in sea-ice nonlinearity (Supplementary Figure 6), Arctic temperature doubling differences averaged across the four extra models align closely with the sea-ice albedo doubling differences (Figure 4b,c), with patterns similar to those for HadGEM2-ES (Figure 2f). Similar comments apply to the evaporation mechanism at lower latitudes (Figure 4d,e; Supplementary Figure 7), especially over the Americas, Africa and Arabia, although not all of the pattern is explained this way (nonlinear dynamical processes and internal variability may also contribute).

The implications of nonlinearity for individual studies will be application-specific, and should be considered alongside other issues, such as impacts model uncertainty. Further differences in patterns of 'potentially-avoidable' and 'unavoidable' warming may arise from linear mechanisms. The abruptCO2 experiments are powerful for separating mechanisms and identifying where nonlinearity is largest or smallest.

Where available, transient projections from state-of-the-art climate models remain preferable for direct policy advice.

Work is needed to reduce uncertainty in these nonlinear mechanisms. Our experimental design could usefully be applied to other models. Some policy advice based on linear methods<sup>3</sup> may need to be reconsidered, while studies of physical processes controlling both temperature and precipitation<sup>25,26</sup> should account for a different balance of mechanisms under different forcing scenarios or for different time periods.

## **Methods**

### **HadGEM2-ES model and experiments**

The Hadley Centre Global Environmental Model version 2 Earth System configuration (HadGEM2-ES)<sup>27,28</sup> has an atmospheric resolution of 1.25x1.875° and 38 vertical levels, and a 1° ocean (reaching 1/3° near the equator) with 40 vertical levels. NCAR CESM1, HadCM3, IPSL CM5A-LR and MIROC5 are described in supplementary Table 2.

All models ran a fixed-forcings pre-industrial control, and both abruptCO<sub>2</sub> experiments. Each abruptCO<sub>2</sub> experiment was initialised from the same point in the control run, and CO<sub>2</sub> was abruptly changed (to twice pre-industrial levels for abrupt2xCO<sub>2</sub> and four times for abrupt4xCO<sub>2</sub>), and then held constant for 150 years.

The hosing experiment, run for HadGEM2-ES only, involved addition of 0.1Sv freshwater near the coast of Greenland for 100 years. This produced a modest (30%) slowdown in the AMOC (measured by maximum overturning near 30N). Results from this experiment were averaged over years 50-149.

### **Scaling the global-mean nonlinearity out of the regional temperature doubling differences**

Figure 2c shows doubling differences after the global-mean nonlinearities (except those due to the AMOC) are scaled out. The calculation of doubling differences with global non-linearities scaled out (denoted  $DD_{noglob}$ ) is described below. The small global-mean nonlinearity associated with the AMOC is not scaled out here. This is because the global-mean AMOC effect is included in Figure 2d (the scaled hosing response), and is therefore removed when Figure 2d is subtracted from Figure 2c: to give the residual in Figure 2e.  $DD_{noglob}$  is given by:

$$DD_{noglob} = T_{42} - T_{21,scaled}$$

where  $T_{42}$  is the warming from the second doubling, and:

$$T_{21,scaled} = T_{21} \cdot \frac{(\overline{T_{21}} + \overline{DD_{noAMOC}})}{\overline{T_{21}}}$$

where  $T_{21}$  is the warming from the first doubling. The overbar indicates a global

287 mean.  $\overline{DD_{noAMOC}}$  is the global mean doubling difference from processes other than  
288 the AMOC:

289

290 
$$\overline{DD_{noAMOC}} = \overline{DD} - \overline{DD_{AMOC}}$$

291

292  $\overline{DD}$  is the global mean of Figure 2a and  $\overline{DD_{AMOC}}$  is the global mean of Figure 2d.

293

294

295

## 296 **References**

297

- 298 1 Arnell, N. W. *et al.* A global assessment of the effects of climate policy on the  
 299 impacts of climate change. *Nat Clim Change* **3**, 512-519, doi:Doi  
 300 10.1038/Nclimate1793 (2013).
- 301 2 Oppenheimer, M. Defining dangerous anthropogenic interference: The role of  
 302 science, the limits of science. *Risk Anal* **25**, 1399-1407, doi:DOI  
 303 10.1111/j.1539-6925.2005.00687.x (2005).
- 304 3 Gosling, S. N. *et al.* A review of recent developments in climate change  
 305 science. Part II: The global-scale impacts of climate change. *Prog Phys Geog*  
 306 **35**, 443-464, doi:Doi 10.1177/0309133311407650 (2011).
- 307 4 Todd, M. C. *et al.* Uncertainty in climate change impacts on basin-scale  
 308 freshwater resources - preface to the special issue: the QUEST-GSI  
 309 methodology and synthesis of results. *Hydrol Earth Syst Sc* **15**, 1035-1046,  
 310 doi:DOI 10.5194/hess-15-1035-2011 (2011).
- 311 5 van Vuuren, D. P. *et al.* How well do integrated assessment models simulate  
 312 climate change? *Climatic Change* **104**, 255-285, doi:DOI 10.1007/s10584-  
 313 009-9764-2 (2011).
- 314 6 Moss, R. H. *et al.* The next generation of scenarios for climate change research  
 315 and assessment. *Nature* **463**, 747-756, doi:Doi 10.1038/Nature08823 (2010).
- 316 7 Huntingford, C. *et al.* Simulated resilience of tropical rainforests to CO2-  
 317 induced climate change. *Nat Geosci* **6**, 268-273, doi:Doi 10.1038/Ngeo1741  
 318 (2013).
- 319 8 Chadwick, R., Wu, P. L., Good, P. & Andrews, T. Asymmetries in tropical  
 320 rainfall and circulation patterns in idealised CO2 removal experiments.  
 321 *Climate Dynamics* **40**, 295-316, doi:DOI 10.1007/s00382-012-1287-2 (2013).
- 322 9 Li, S. & Jarvis, A. Long run surface temperature dynamics of an A-OGCM:  
 323 the HadCM3 4xCO(2) forcing experiment revisited. *Climate Dynamics* **33**,  
 324 817-825, doi:10.1007/s00382-009-0581-0 (2009).
- 325 10 Manabe, S., Bryan, K. & Spelman, M. J. Transient-Response of a Global  
 326 Ocean Atmosphere Model to a Doubling of Atmospheric Carbon-Dioxide. *J*  
 327 *Phys Oceanogr* **20**, 722-749, doi:Doi 10.1175/1520-  
 328 0485(1990)020<0722:Troago>2.0.Co;2 (1990).
- 329 11 Meinshausen, M. *et al.* The RCP greenhouse gas concentrations and their  
 330 extensions from 1765 to 2300. *Climatic Change* **109**, 213-241, doi:DOI  
 331 10.1007/s10584-011-0156-z (2011).
- 332 12 Good, P., Gregory, J. M. & Lowe, J. A. A step-response simple climate model  
 333 to reconstruct and interpret AOGCM projections. *Geophysical Research*  
 334 *Letters* **38**, -, doi:Artn L01703  
 335 Doi 10.1029/2010gl045208 (2011).
- 336 13 Good, P., Gregory, J. M., Lowe, J. A. & Andrews, T. Abrupt CO2  
 337 experiments as tools for predicting and understanding CMIP5 representative  
 338 concentration pathway projections. *Climate Dynamics* **40**, 1041-1053, doi:DOI  
 339 10.1007/s00382-012-1410-4 (2013).
- 340 14 Andrews, T. & Ringer, M. A. Cloud Feedbacks, Rapid Adjustments, and the  
 341 Forcing-Response Relationship in a Transient CO2 Reversibility Scenario.  
 342 *Journal of Climate* **27**, 1799-1818, doi:Doi 10.1175/Jcli-D-13-00421.1 (2014).



343 15 Jonko, A. K., Shell, K. M., Sanderson, B. M. & Danabasoglu, G. Climate  
344 Feedbacks in CCSM3 under Changing CO<sub>2</sub> Forcing. Part II: Variation of  
345 Climate Feedbacks and Sensitivity with Forcing. *Journal of Climate* **26**, 2784-  
346 2795, doi:Doi 10.1175/Jcli-D-12-00479.1 (2013).

347 16 Colman, R. & McAvaney, B. Climate feedbacks under a very broad range of  
348 forcing. *Geophysical Research Letters* **36**, doi:L01702  
349 10.1029/2008gl036268 (2009).

350 17 Hansen, J. *et al.* Efficacy of climate forcings. *Journal of Geophysical*  
351 *Research-Atmospheres* **110**, 45, doi:D18104  
352 10.1029/2005jd005776 (2005).

353 18 Ishizaki, Y. *et al.* Temperature scaling pattern dependence on representative  
354 concentration pathway emission scenarios. *Climatic Change* **112**, 535-546,  
355 doi:DOI 10.1007/s10584-012-0430-8 (2012).

356 19 Drijfhout, S. S., Weber, S. L. & van der Swaluw, E. The stability of the MOC  
357 as diagnosed from model projections for pre-industrial, present and future  
358 climates. *Climate Dynamics* **37**, 1575-1586, doi:DOI 10.1007/s00382-010-  
359 0930-z (2011).

360 20 Hall, A. The role of surface albedo feedback in climate. *Journal of Climate* **17**,  
361 1550-1568, doi:Doi 10.1175/1520-0442(2004)017<1550:Trosaf>2.0.Co;2  
362 (2004).

363 21 Eisenman, I. Factors controlling the bifurcation structure of sea ice retreat.  
364 *Journal of Geophysical Research-Atmospheres* **117**, doi:Artn D01111  
365 Doi 10.1029/2011jd016164 (2012).

366 22 Seneviratne, S. I. *et al.* Investigating soil moisture-climate interactions in a  
367 changing climate: A review. *Earth-Sci Rev* **99**, 125-161, doi:DOI  
368 10.1016/j.earscirev.2010.02.004 (2010).

369 23 Seneviratne, S. I., Luthi, D., Litschi, M. & Schar, C. Land-atmosphere  
370 coupling and climate change in Europe. *Nature* **443**, 205-209, doi:Doi  
371 10.1038/Nature05095 (2006).

372 24 Field, C. B., Jackson, R. B. & Mooney, H. A. Stomatal Responses to Increased  
373 Co<sub>2</sub> - Implications from the Plant to the Global-Scale. *Plant Cell Environ* **18**,  
374 1214-1225, doi:DOI 10.1111/j.1365-3040.1995.tb00630.x (1995).

375 25 Chadwick, R. & Good, P. Understanding non-linear tropical precipitation  
376 responses to CO<sub>2</sub> forcing. *Geophysical Research Letters* **40**,  
377 doi:10.1002/grl.50932 (2013).

378 26 Good, P. *et al.* A step-response approach for predicting and understanding  
379 non-linear precipitation changes. *Climate Dynamics* **39**, 2789-2803, doi:DOI  
380 10.1007/s00382-012-1571-1 (2012).

381 27 Collins, W. J. *et al.* Development and evaluation of an Earth-System model –  
382 HadGEM2. *Geophysical Model Development (submitted)* (2011).

383 28 Martin, G. M. *et al.* The HadGEM2 family of Met Office Unified Model  
384 climate configurations. *Geosci Model Dev* **4**, 723-757, doi:DOI 10.5194/gmd-  
385 4-723-2011 (2011).

386

387

388

389

## 390 ***Acknowledgements***

391

392 This work was supported by the Joint UK DECC/Defra Met Office Hadley Centre  
393 Climate Programme (GA01101). NB and JMG received funding from the European  
394 Research Council under the European Community's Seventh Framework Programme  
395 (FP7/2007-2013), ERC Grant Agreement 247220, project "Seachange." Simulations  
396 by J.L.D. were done as part of the ANR ClimaConf project (grant #ANR-10-CEPL-  
397 0003). HS was supported by the SOUSEI program from the Ministry of Education,  
398 Culture, Sports, Science and Technology of Japan and the Environment Research and  
399 Technology Development Fund (S-10) of the Ministry of the Environment of Japan.  
400 NS was supported by the Swiss National Science Foundation.

401

## 402 ***Author contributions***

403

404 P.G. conceived the study and wrote the paper. All authors contributed to the scientific  
405 interpretation and the paper. T.A., M.B.M, J.L.D., J.M.G., N.S. and H.S. performed  
406 experiments.

407

## 408 ***Competing financial interests statement***

409

410 The authors have no competing interests as defined by Nature Publishing Group, or  
411 other interests that might be perceived to influence the results and/or discussion  
412 reported in this article.

413

414

## **Figure legends**

Figure 1. Regional nonlinearity in the transient-forced 1pctCO<sub>2</sub> experiment.

Warming (K) simulated directly by HadGEM2-ES (y-axis) is compared with that predicted from the linear reconstruction<sup>12,13</sup> using (left column) abrupt2xCO<sub>2</sub> and (right column) abrupt4xCO<sub>2</sub> responses. Good performance of the linear reconstruction is indicated by the points lying close to the red line (each point represents one model grid cell). Results are averaged over (top row) years 120-139 of the 1pctCO<sub>2</sub> experiment (near 4xCO<sub>2</sub>), and (bottom row) years 61-80 (near 2xCO<sub>2</sub>).

Figure 2. Mechanisms of nonlinear regional warming in HadGEM2-ES. Left column: doubling differences (K); a) unscaled; c) after global-mean nonlinearity is scaled out (Methods); e) as c), but with nonlinearity associated with the AMOC (panel d) subtracted; g) as e) but latitude range matches that of panel h). b) doubling ratio. d) estimated nonlinearity associated with the AMOC. f) doubling difference in sea ice fraction. h) Bowen ratio at 4xCO<sub>2</sub> divided by Bowen ratio at 2xCO<sub>2</sub>. All based on means over years 50-149 of the abrupt2xCO<sub>2</sub>, abrupt4xCO<sub>2</sub> or hosing experiments.

Figure 3. Doubling ratio of ensemble mean warming. Ensemble means are taken for each of the first and second CO<sub>2</sub> doublings first, then the doubling ratio calculated.

Figure 4. Multi-model mechanisms of temperature nonlinearity. All panels: 'scaled temperature doubling differences' have had the global mean nonlinearity scaled out. a) AMOC influence, averaged over NW Europe (land, 10W-20E, 45-70N). Y-axis: scaled temperature doubling difference for each model; x-axis: the HadGEM2-ES

hosing temperature response scaled using the doubling difference in AMOC index for  
each model (as Figure 2d; Pink: HadGEM2-ES; dark blue: HadCM3; light blue:  
MIROC5; yellow: NCAR CESM1; red: IPSL CM5A-LR). b,c) Sea-ice influence.  
Ensemble means (excluding HadGEM2), of b: scaled temperature doubling difference  
and c: albedo doubling difference. d,e) Evaporation influence. d: Ensemble mean  
(excluding HadGEM2) scaled temperature doubling difference; e: Bowen ratio of  
ensemble mean surface heat fluxes at 4xCO<sub>2</sub>, divided by the equivalent at 2xCO<sub>2</sub> (as  
Figure 2h).

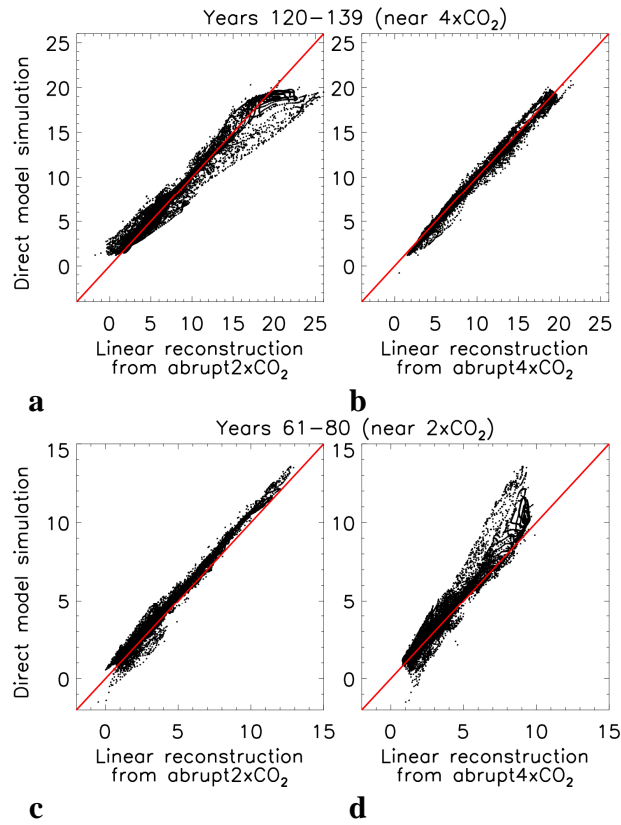


Figure 1. Regional nonlinearity in the transient-forced 1pctCO<sub>2</sub> experiment. Warming (K) simulated directly by HadGEM2-ES (y-axis) is compared with that predicted from the linear reconstruction<sup>12,13</sup> using (left column) abrupt2xCO<sub>2</sub> and (right column) abrupt4xCO<sub>2</sub> responses. Good performance of the linear reconstruction is indicated by the points lying close to the red line (each point represents one model grid cell). Results are averaged over (top row) years 120-139 of the 1pctCO<sub>2</sub> experiment (near 4xCO<sub>2</sub>), and (bottom row) years 61-80 (near 2xCO<sub>2</sub>).

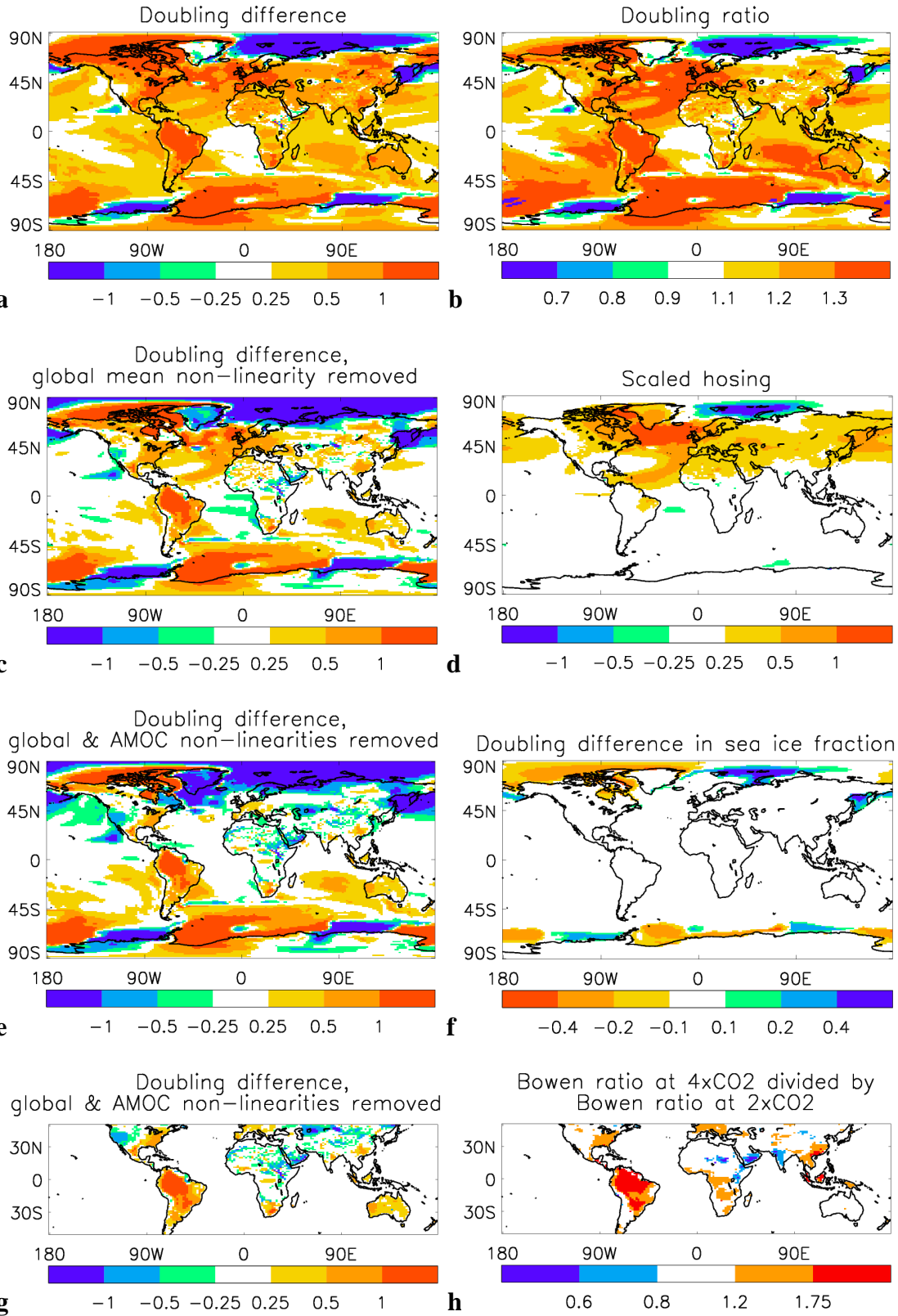


Figure 2. Mechanisms of nonlinear regional warming in HadGEM2-ES. Left column: doubling differences (K); a) unscaled; c) after global-mean nonlinearity is scaled out (Methods); e) as c), but with nonlinearity associated with the AMOC (panel d) subtracted; g) as e) but latitude range matches that of panel h). b) doubling ratio. d) estimated nonlinearity associated with the AMOC. f) doubling difference in sea ice

fraction. h) Bowen ratio at  $4\times\text{CO}_2$  divided by Bowen ratio at  $2\times\text{CO}_2$ . All based on means over years 50-149 of the abrupt $2\times\text{CO}_2$ , abrupt $4\times\text{CO}_2$  or hosing experiments.

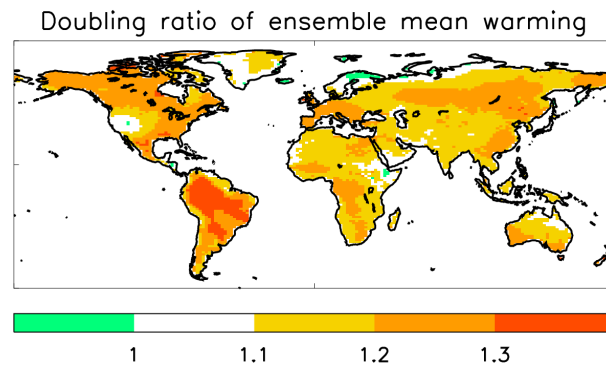
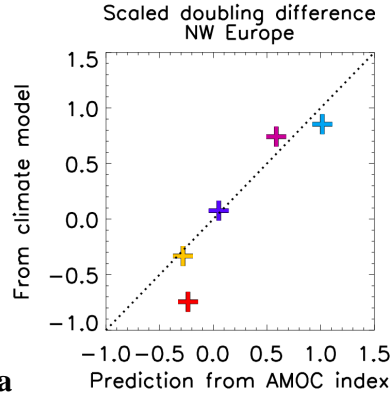


Figure 3. Doubling ratio of ensemble mean warming. Ensemble means are taken for each of the first and second  $\text{CO}_2$  doublings first, then the doubling ratio calculated.

493



494

**a**

495

Mean scaled temperature doubling difference/K



**b**

496

497

Mean albedo doubling difference

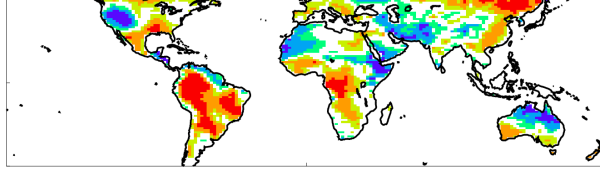


**c**

498

499

Mean scaled temperature doubling difference/K

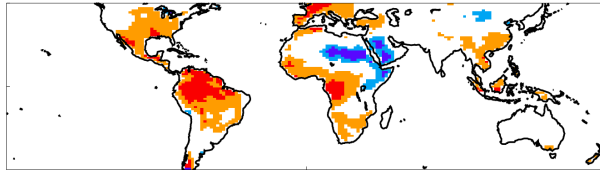


**d**

500

501

(Bowen ratio at 4xCO<sub>2</sub>)/(Bowen ratio at 2xCO<sub>2</sub>)



**e**

502

503

504

Figure 4. Multi-model mechanisms of temperature nonlinearity. All panels: ‘scaled temperature doubling differences’ have had the global mean nonlinearity scaled out. a) AMOC influence, averaged over NW Europe (land, 10W-20E, 45-70N). Y-axis: scaled temperature doubling difference for each model; x-axis: the HadGEM2-ES hosing temperature response scaled using the doubling difference in AMOC index for each model (as Figure 2d; Pink: HadGEM2-ES; dark blue: HadCM3; light blue: MIROC5; yellow: NCAR CESM1; red: IPSL CM5A-LR). b,c) Sea-ice influence. Ensemble means (excluding HadGEM2), of b: scaled temperature doubling difference and c: albedo doubling difference. d,e) Evaporation influence. d: Ensemble mean (excluding HadGEM2) scaled temperature doubling difference; e: Bowen ratio of



515 ensemble mean surface heat fluxes at  $4xCO_2$ , divided by the equivalent at  $2xCO_2$  (as  
516 Figure 2h).

517

518

519

520

# **Supplementary material for ‘Nonlinear regional warming at higher CO<sub>2</sub> concentrations’**

**Peter Good<sup>1</sup>, Jason A. Lowe<sup>1</sup>, Timothy Andrews<sup>1</sup>, Andrew Wiltshire<sup>1</sup>, Robin  
Chadwick<sup>1</sup>, Jeff K Ridley<sup>1</sup>, Matthew B Menary<sup>1</sup>, Nathaëlle Bouttes<sup>2</sup>, Jean Louis  
Dufresne<sup>3</sup>, Jonathan M Gregory<sup>2,1</sup>, Nathalie Schaller<sup>4,5</sup>, Hideo Shiogama<sup>6</sup>**

<sup>1</sup> Met Office Hadley Centre, Exeter, United Kingdom

<sup>2</sup> NCAS-Climate, University of Reading, Reading, United Kingdom

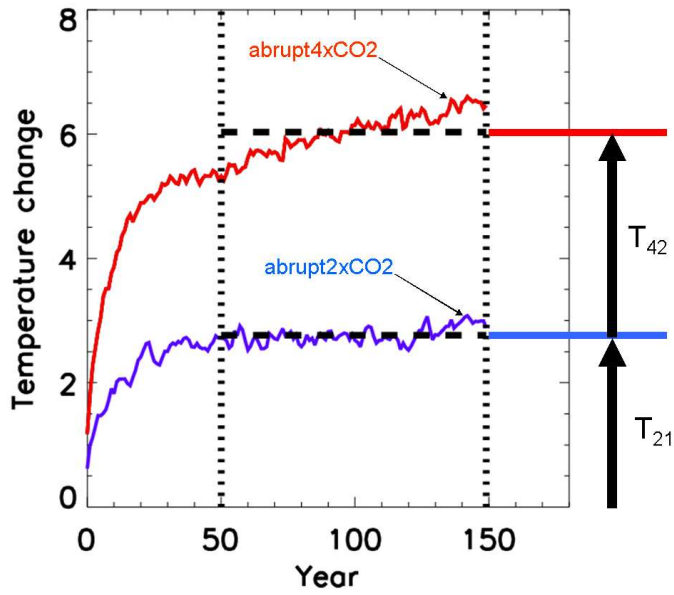
<sup>3</sup> Laboratoire de Météorologie Dynamique, Institut Pierre Simon Laplace,  
Paris, France

<sup>4</sup> Institute for Atmospheric and Climate Science, Department of Environmental Sciences,  
Swiss Federal Institute of Technology, Zurich, Switzerland

<sup>5</sup> Atmospheric, Oceanic and Planetary Physics, University of Oxford, Parks Road, Oxford  
OX1 3PU, United Kingdom

<sup>6</sup> Climate Risk Assessment Section, Centre for Global Environmental Research,  
National Institute for Environmental Studies, Japan

*To be submitted to Nature Climate Change*



Supplementary Figure 1. Illustrating the doubling difference and doubling ratio calculations. The main results are averaged over years 50-149 – see vertical dotted lines. The red and blue curves show global mean warming timeseries for illustration. The doubling difference is given by  $T_{42} - T_{21}$ , the doubling ratio by  $T_{42} / T_{21}$ .

## **1. Interpreting averages over years 50-149 of the abruptCO2 experiments**

Our analysis focuses on averages over years 50-149 of each abruptCO2 experiment. This section discusses how these results may approximately be related to policy-relevant scenario projections. This does not mean that the results are substitutes for scenario projections (in particular, the distinct effects of non-CO2 forcings are absent): it just gives a rough context. The main paper states that, "For abrupt2xCO2, these 100-year means may roughly be interpreted as the results for year 2100 of a CO2-only version of rcp4.5." This statement arises from the method behind Figure 1, as follows.

Supplementary Figure 2 shows the timeseries of global mean radiative forcing for rcp4.5 (blue). It also shows an idealised transient scenario (black line) that is roughly similar to rcp4.5. We show below that the mean over years 50-149 of the abrupt2xCO2 experiment represents an estimate of the response at year 2100 of the scenario represented by the black line.

As demonstrated in the main paper (Figures 1b,c) and in previous literature<sup>1-3</sup>, it is possible to use a simple linear combination of abruptCO2 responses to estimate climate change under a transient forcing experiment. This method works well (Figures 1b,c) when it is used to simulate periods in the transient experiment when the forcing matches that of the abruptCO2 experiment.

The method we use to estimate the response to a transient experiment from an abruptCO2 experiment is a linear response function approach. It is given simply by the following equation:

$$y_i = \sum_{j=0}^i \frac{\Delta F_{i-j}}{\Delta F_a} x_j \quad \text{supplementary equation 1}$$

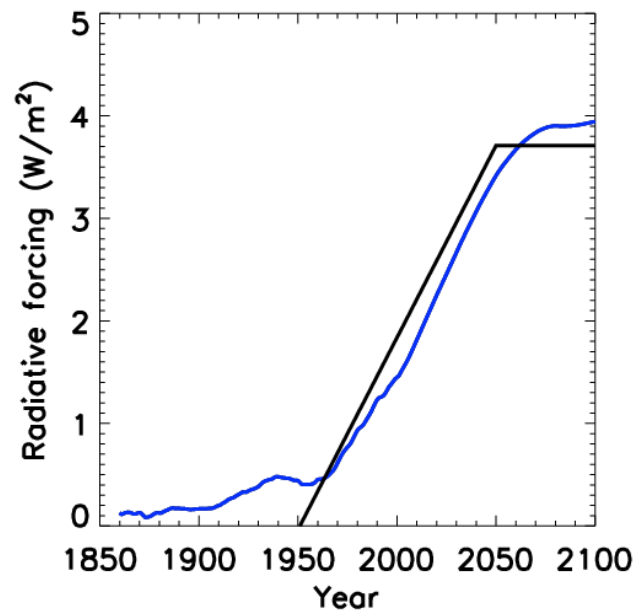
where  $y_i$  is the estimated transient temperature response at year  $i$  and  $x_j$  is the temperature response at year  $j$  of the CO<sub>2</sub> step experiment.  $\Delta F_{i-j}$  is the annual step change in radiative forcing during year  $i-j$  of the scenario.  $\Delta F_a$  is the radiative forcing change in the abruptCO<sub>2</sub> experiment. (Essentially, this treats the transient scenario as a series of small annual step changes in forcing: the response to each step is estimated by scaling the abruptCO<sub>2</sub> response).

The black line in Supplementary Figure 2 represents an experiment where CO<sub>2</sub> is increased by 0.7% per year for 100 years, then held constant for 50 years (reaching a peak CO<sub>2</sub> concentration of double the pre-industrial level). This corresponds to an approximately constant rate of forcing increase during the ramp-up period. As this experiment takes 100 years to double CO<sub>2</sub>, the annual change in forcing is equal to the abrupt2xCO<sub>2</sub> forcing divided by 100. Therefore, the ratio  $\Delta F_{i-j} / \Delta F_a$  is set equal to 1/100 for the first 100 years (i.e. for  $i-j \leq 99$  in supplementary equation 1); and equal to zero for the last 50 years (i.e. for  $i-j > 99$ ). To obtain the warming at the end of the scenario, we set  $i=149$  (the scenario is 150 years long). Therefore,  $\Delta F_{i-j} / \Delta F_a$  is equal to 1/100 for  $j \geq 50$ ; and equal to zero for  $j < 50$ . Using supplementary

equation 1, therefore, the response at the end of this experiment may be estimated from the abrupt2xCO2 response as follows:

$$y = \sum_{j=50}^{149} \frac{1}{100} x_j^{(abrupt2xCO2)} \quad \text{supplementary equation 2}$$

(The summation starts from j=50 because  $\Delta F_{i-j} / \Delta F_a$  is zero for j < 50). This is simply equal to the mean over years 50-149 of the abrupt2xCO2 experiment – as used in the main paper.



Supplementary Figure 2. Total global-mean radiative forcing timeseries. Blue: for rcp4.5, as estimated by the IAM used to produce the scenario forcing dataset<sup>4</sup> (from the RCP database: <http://www.iiasa.ac.at/web-apps/tnt/RcpDb>). Black: for a scenario where CO2 is increased by 0.7% per year for 100 years, then stabilised for 50 years.

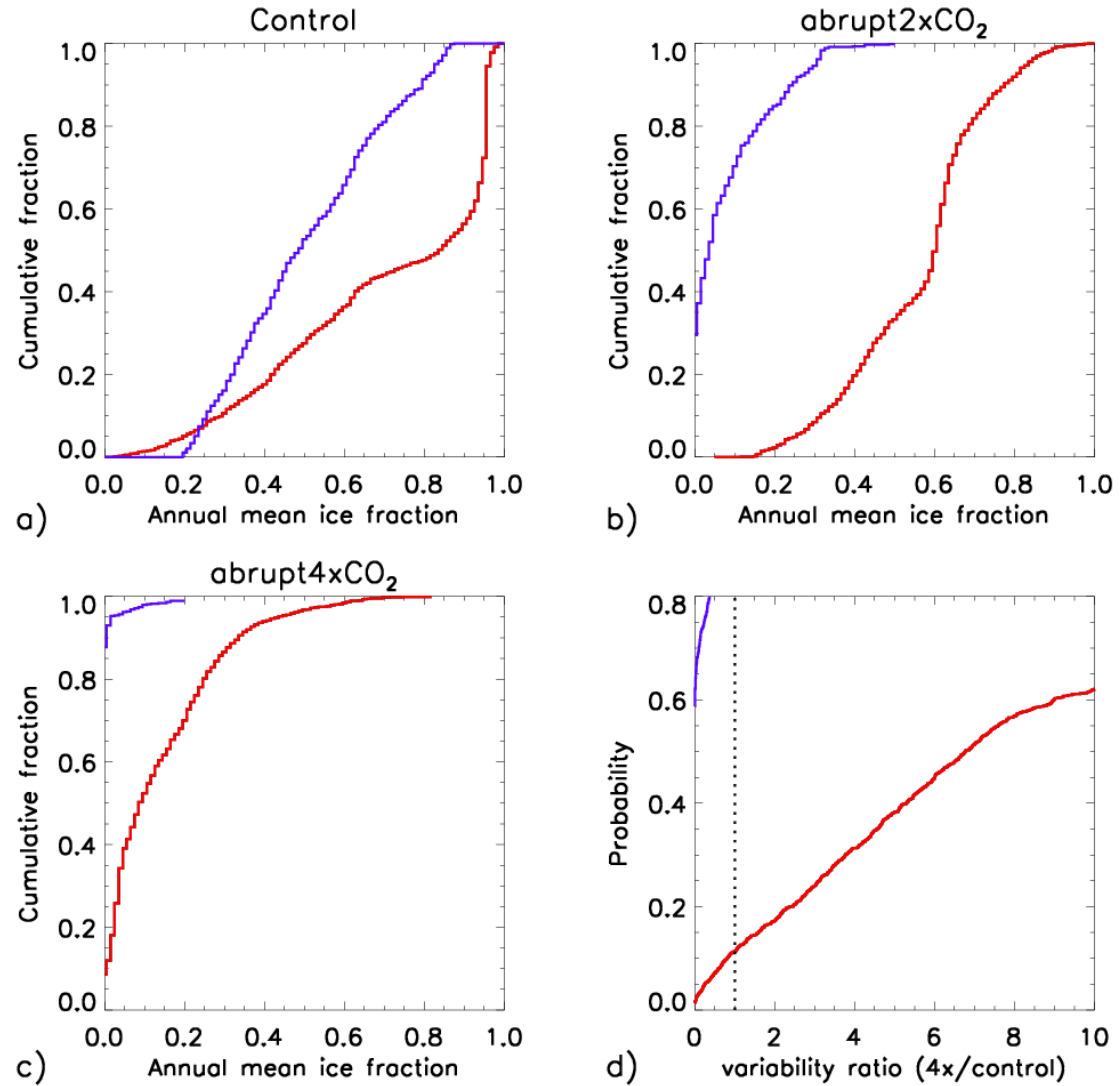
## **1. Sea-ice non-linearity in HadGEM2-ES**

The patterns of temperature nonlinearities over high latitude oceans (Figure 2e) correspond closely to nonlinearities in sea-ice cover (Figure 2f). The scale in Figure 2f is reversed, because reductions in sea-ice cover tend to drive increases in warming. Here we provide support for the nonlinear albedo feedback being a prominent driver of high-latitude temperature non-linearity..

Supplementary figure 3 shows statistics of the climatological mean and interannual variability in sea-ice fraction. The blue(red) lines show results when only regions with sea-ice doubling difference larger than 0.2(smaller than -0.2) are included. Climate means are shown for the control and each abruptCO<sub>2</sub> experiment (panels a-c). Panel d shows the ratio in variability between the abrupt4xCO<sub>2</sub> experiment and the control. Regions with positive nonlinearities in sea ice cover (with doubling difference > 0.2; c.f. Figure 2f) have intermediate ice cover in the control experiment (Supplementary figure 3a, blue line), but (near) zero ice cover in the abrupt4xCO<sub>2</sub> experiment (supplementary figure 3c, blue line). Correspondingly, the interannual variability in ice cover is much lower at 4xCO<sub>2</sub> than in the control (supplementary figure 3d, blue line). This is consistent with the idea of smaller albedo feedback at 4xCO<sub>2</sub> due to a transition from intermediate to negligible ice cover.

Regions with negative sea ice nonlinearities (doubling difference < -0.2) have much larger sea ice variability at 4xCO<sub>2</sub> than in the control (supplementary figure 3d, red line), and often have large ice cover in the control (supplementary figure 3a), and non-

zero cover even at 4xCO<sub>2</sub> (supplementary figure 3c). This is consistent with the idea of albedo feedback being higher in the abrupt4xCO<sub>2</sub> experiment.



Supplementary figure 3. Statistics of sea-ice mean (a-c) and variability (d) for regions with (blue) sea-ice doubling difference > 0.2 and (red) sea-ice doubling difference < -0.2. Panel d) shows the ratio: (variability in abrupt4xCO<sub>2</sub>)/(variability in control), where variability is quantified as the standard deviation in annual mean sea-ice cover over years 50-149 of each experiment.



## **2. Evaporation over the Amazon in HadGEM2-ES**

The large temperature non-linearities over the Amazon are associated with a substantially larger Bowen ratio at 4xCO<sub>2</sub> compared to 2xCO<sub>2</sub> (Figure 2h). Here we link this to reduced forest tree stomatal conductance at higher CO<sub>2</sub>, driven by a direct stomatal response to CO<sub>2</sub>, with a secondary effect due to reduced photosynthesis at high temperature. We show results averaged over the western Amazon (72-60W, 12S-3N), capturing the main temperature non-linearity.

Over this region, latent heat flux from evaporation is significantly lower in the abrupt4xCO<sub>2</sub> experiment than in the abrupt2xCO<sub>2</sub> experiment (supplementary figure 4a; blue: abrupt2xCO<sub>2</sub>; red: abrupt4xCO<sub>2</sub>). The total turbulent heat flux is relatively similar in the two experiments (supplementary figure 4b), so the decrease in latent heat flux is balanced by a corresponding increase in sensible heat flux (supplementary figure 4c). This is consistent with the idea of restricted evaporation causing a larger proportion of surface heat to be lost by sensible heat, with a corresponding increase in surface temperature.

Surface evaporation is determined by atmospheric demand divided by net resistance<sup>5</sup>. The net resistance quantifies limitations on water supply, accounting for soil moisture, biophysical control by plants (via stomata) and the process of transferring moisture from the surface to the lowest atmospheric layer. The decrease in evaporation (at 4xCO<sub>2</sub> compared to 2xCO<sub>2</sub>) is driven by a relatively large (around 35%) decrease in

1/(net resistance) – see Supplementary figure 4d. We plot 1/(net resistance), because evaporation is proportional to 1/(net resistance), at constant atmospheric demand. This decrease in 1/(net resistance) is dominated by a decrease in stomatal conductance associated with the broadleaf tropical forest trees: supplementary figure 4e shows changes due to stomatal conductance alone, and is similar to supplementary figure 4d.

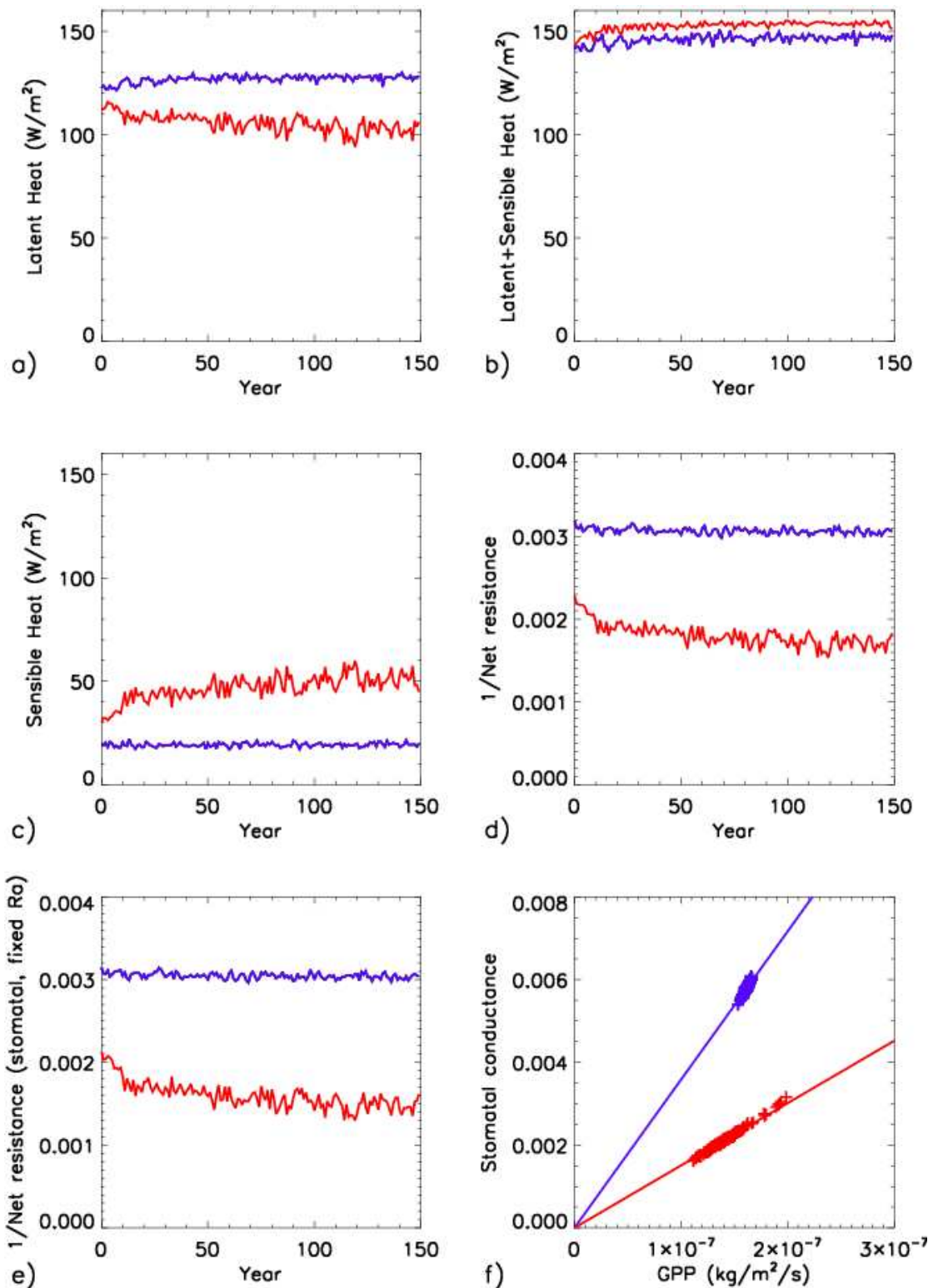
The difference in stomatal conductance between the two experiments (seen in supplementary figure 4e) is largely due to a fast response of stomata to the different CO<sub>2</sub> levels. This appears in supplementary figure 4e as a difference between the red and blue lines present from the first year. Moisture stress is negligible for forest trees in this region in both experiments (not shown), so regional evaporation is independent of precipitation change.

The subsequent decline in conductance in the abrupt4xCO<sub>2</sub> experiment (supplementary figure 4e, red line) is driven in this model primarily by a decrease in photosynthesis, with stomata closing to maintain near constant leaf internal CO<sub>2</sub> concentration. Evidence for this is given in supplementary figure 4f. This shows that a near constant proportionality is maintained between stomatal conductance and gross primary productivity (GPP, a proxy for photosynthesis, as leaf area is almost constant in this region for these runs). The relationship between photosynthesis and stomatal conductance arises through the transport of carbon through a leaf, which is quantified by the following equation<sup>6</sup>:

$$A = \frac{g_s (c_c - c_i)}{1.6RT^*}$$

179  $A$  is the leaf photosynthesis rate,  $g_s$  the stomatal conductance,  $(c_c - c_i)$  is the  $\text{CO}_2$   
180 concentration gradient across the stomata,  $R$  the perfect gas constant and  $T^*$  the leaf  
181 surface temperature in K (the latter is relatively constant in these runs as it is in units  
182 of K). The near-constant proportionality between stomatal conductance and  
183 photosynthesis (supplementary figure 4f, red line) means that  $(c_c - c_i)$  is  
184 approximately constant. That is, the model of stomatal conductance in HadGEM2-ES  
185 acts to keep the internal leaf  $\text{CO}_2$  concentration ( $c_i$ ) roughly constant during the  
186 abrupt4x $\text{CO}_2$  experiment ( $c_c$ , the external  $\text{CO}_2$  concentration is approximately  
187 constant during the abrupt4x $\text{CO}_2$  run). It does this by closing stomata (decreasing  $g_s$ ),  
188 which in turn reduces water loss.

190 Large uncertainties exist in the modelling of stomatal responses to  $\text{CO}_2$  increase<sup>7</sup>.  
191 HadGEM2-ES does not include photosynthetic acclimation<sup>8</sup>, which could reduce the  
192 decrease in GPP at high temperature, potentially reducing the decreases in stomatal  
193 conductance. However, the magnitude of this effect is highly uncertain<sup>9</sup>.

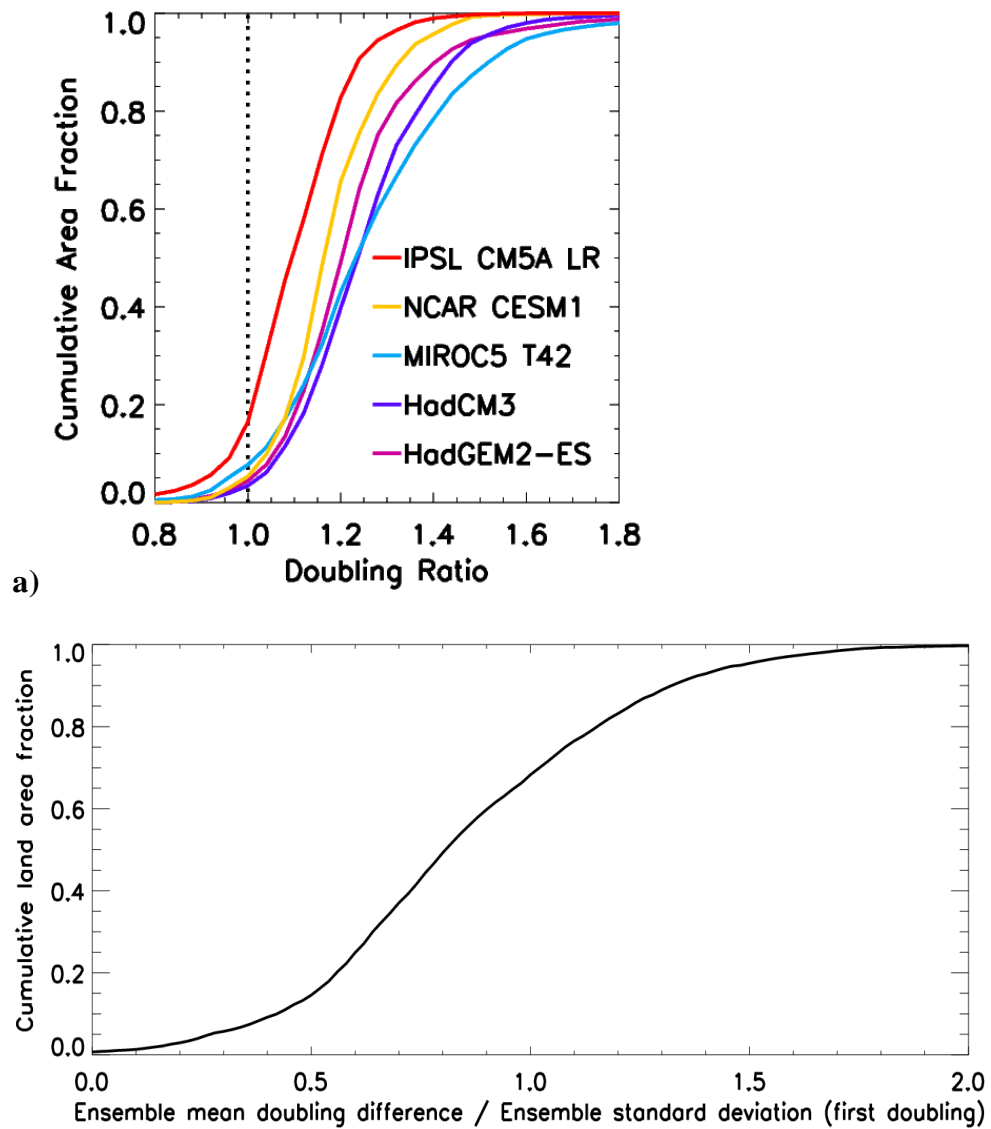


197

198 Supplementary figure 4. Diagnostics relating to evaporation, averaged over the  
 199 Western Amazon, for the abrupt2xCO<sub>2</sub> (blue) and abrupt4xCO<sub>2</sub> (red) experiments.

200 See text for description.

### 3. Multi-model statistics of nonlinearity over land



Supplementary Figure 5. a) Cumulative area distribution functions of the temperature doubling ratio over land, for each model. b) Cumulative area distribution function of the ratio: (ensemble mean doubling difference) / (Ensemble standard deviation from the first doubling).

#### 213 **4. Inflation in model spread for the second CO<sub>2</sub> doubling**

214  
215 The main paper reports that, over about 30% of the land area, the model spread in  
216 warming per K of global warming is more than 1.4 times larger for the second  
217 doubling than for the first. In this section, we will address the possibility of the  
218 inflation of model spread being an artifact of internal variability.

219  
220 A difference in the standard deviation between two datasets can arise simply from  
221 internal variability. This is because the climate state for each model is estimated from  
222 the mean over a finite period. Even though 100-year means are used in this study,  
223 internal variability may still play a role.

224  
225 We denote the ratio between the standard deviation for the second doubling, and that  
226 for the first, as R:

$$228 \quad R = \frac{\sigma_{42}}{\sigma_{21}},$$

229 where  $\sigma_{42}$ , the ensemble standard deviation for the second doubling (where CO<sub>2</sub>  
230 changes from 2x to 4x pre-industrial levels) is given by:

$$232 \quad \sigma_{42} = \sqrt{V_{42}^{(m)} + V_4^{(i)} + V_2^{(i)}},$$

233  
234 where  $V_{42}^{(m)}$  is the variance due to model differences alone;  $V_4^{(i)}$  is the variance from  
235 internal variability in the climate at 4xCO<sub>2</sub>; and  $V_2^{(i)}$  the equivalent at 2xCO<sub>2</sub>.

236 Similarly,  $\sigma_{21}$ , the standard deviation for the first doubling, is given by:

237

238 
$$\sigma_{21} = \sqrt{V_{21}^{(m)} + V_2^{(i)} + V_1^{(i)}}$$

239

240 Therefore, R is given by:

241

242 
$$R = \frac{\sqrt{V_{42}^{(m)} + V_4^{(i)} + V_2^{(i)}}}{\sqrt{V_{21}^{(m)} + V_2^{(i)} + V_1^{(i)}}}$$

243

244  $V_2^{(i)}$  appears on both top and bottom of this ratio. This means that if  $V_2^{(i)}$  was much  
245 larger than the other variances, R would tend to 1 everywhere. This cannot explain  
246 our finding of large areas with  $R > 1.4$ .

247

248 If  $V_4^{(i)}$  (the internal variability in the mean at 4xCO<sub>2</sub>) was increased, however, R  
249 would increase everywhere (and so the area with  $R > 1.4$  would increase). We tested  
250 the importance of  $V_4^{(i)}$  by artificially increasing it: by calculating the climate means  
251 for abrupt4xCO<sub>2</sub> using shorter averaging periods (but centred on the same year as the  
252 100-year means). This has minimal effect on our result: the fraction of land with  $R >$   
253 1.4 is still 32% even if this averaging period is reduced to 20 years (compared to 30%  
254 for 100 year means). This suggests that, for the 100-year means used in the main  
255 paper, internal variability has minimal effect on our estimate for the area with  $R > 1.4$

256

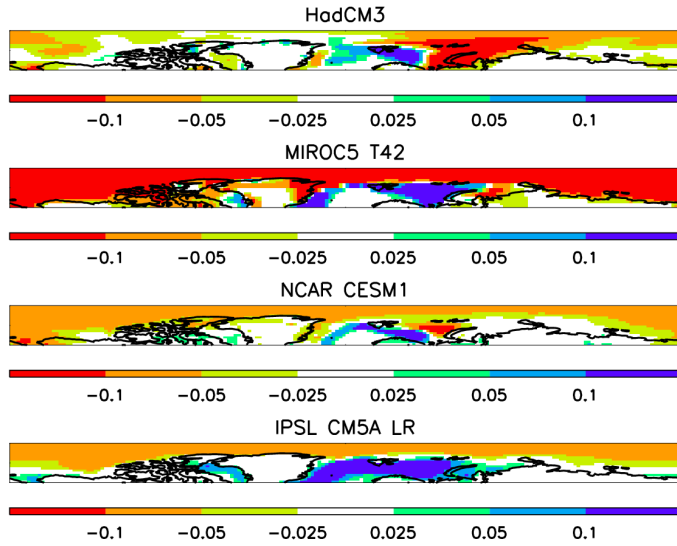
258

## **5. Drivers of nonlinearity from individual models**

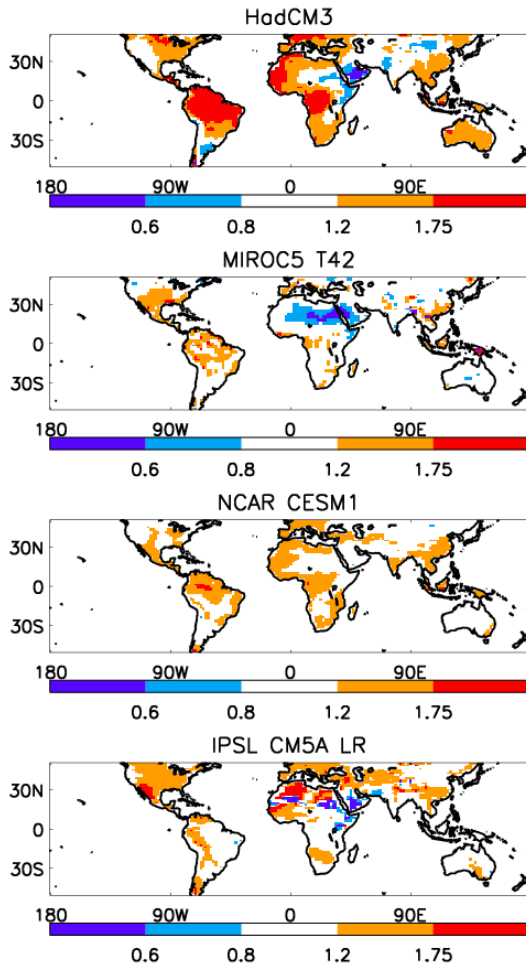
The main paper (Figure 4) shows results for the albedo and evapotranspiration drivers averaged over the four additional climate models (NCAR-CESM1, IPSL CM5A-LR, MIROC5 T42 and HadCM3). Here we show results for individual models (Supplementary Figures 6,7). We also give doubling ratios for global-mean warming (Supplementary Table 1). The spread in the AMOC nonlinearity is illustrated in Figure 4a of the main paper.

As reported in the main paper, the patterns in albedo and evapotranspiration drivers show significant spread across the models. Therefore, their contribution to the overall uncertainty in warming for the second doubling may be substantial in the relevant regions (see discussion on how nonlinearity influences uncertainty in the main paper). The spread in the albedo driver (Supplementary Figure 6) may partly be associated with errors in simulated pre-industrial sea-ice cover (we show above that the sign of the nonlinearity is linked with the control sea-ice cover), so there may be potential for reducing uncertainty using observations. Similarly, the spread in the evapotranspiration driver (Supplementary Figure 7) may partly be associated with errors in pre-industrial soil moisture.





Supplementary Figure 6. Albedo doubling differences: as Figure 4c of the main paper, but for individual models.



Supplementary Figure 7. Bowen ratio of ensemble mean surface heat fluxes at  $4\times\text{CO}_2$ , divided by the equivalent at  $2\times\text{CO}_2$ : as Figure 4e but for each model.

Model	Doubling ratio in global mean warming
NCAR CESM1	1.21
IPSL CM5A-LR	1.05
MIROC5 T42	1.27
HadCM3	1.19
HadGEM2-ES	1.18

Supplementary Table 1. Doubling ratio in global-mean warming for each model.

## 5. Model descriptions

Model and citation	Resolution	Citation
NCAR CESM1 <sup>10</sup>	0.9° longitude x 1.25° latitude, 26 vertical levels	Gent et al., 2011
IPSL CM5A-LR <sup>11</sup>	3.75° longitude x 1.875° latitude, 39 vertical levels	Dufresne et al., 2013
MIROC5 T42 <sup>12</sup>	T42, 40 vertical levels	Watanabe et al., 2010
HadCM3 <sup>13,14</sup>	3.75° longitude x 2.5° latitude, 19 vertical levels	Gordon et al., 2000, Pope et al., 2000

Supplementary Table 2. Descriptions of models used (HadGEM2-ES is described in Methods of main text).

296 **References**

297

298

299 1 Good, P., Gregory, J. M. & Lowe, J. A. A step-response simple climate model  
 300 to reconstruct and interpret AOGCM projections. *Geophysical Research*  
 301 *Letters* **38**, -, doi:Artn L01703

302 Doi 10.1029/2010gl045208 (2011).

303 2 Good, P., Gregory, J. M., Lowe, J. A. & Andrews, T. Abrupt CO2  
 304 experiments as tools for predicting and understanding CMIP5 representative  
 305 concentration pathway projections. *Climate Dynamics* **40**, 1041-1053, doi:DOI  
 306 10.1007/s00382-012-1410-4 (2013).

307 3 Chadwick, R., Wu, P. L., Good, P. & Andrews, T. Asymmetries in tropical  
 308 rainfall and circulation patterns in idealised CO2 removal experiments.  
 309 *Climate Dynamics* **40**, 295-316, doi:DOI 10.1007/s00382-012-1287-2 (2013).

310 4 Meinshausen, M. *et al.* The RCP greenhouse gas concentrations and their  
 311 extensions from 1765 to 2300. *Climatic Change* **109**, 213-241, doi:DOI  
 312 10.1007/s10584-011-0156-z (2011).

313 5 Seneviratne, S. I. *et al.* Investigating soil moisture-climate interactions in a  
 314 changing climate: A review. *Earth-Sci Rev* **99**, 125-161, doi:DOI  
 315 10.1016/j.earscirev.2010.02.004 (2010).

316 6 Cox, P. M. Description of the TRIFFID Dynamic Global Vegetation Model.  
 317 *Technical Note 24, Hadley Centre, Met Office*, 17 pp. (2001).

318 7 Rammig, A. *et al.* Estimating the risk of Amazonian forest dieback. *New*  
 319 *Phytol* **187**, 694-706, doi:DOI 10.1111/j.1469-8137.2010.03318.x (2010).

320 8 Berry, J. A. & Bjorkman, O. Photosynthetic response and adaptation to  
 321 temperature in higher plants. *Annual Review of Plant Physiology* **31**, 491-543  
 322 (1980).

323 9 Smith, N. G. & Dukes, J. S. Plant respiration and photosynthesis in global-  
 324 scale models: incorporating acclimation to temperature and CO2. *Glob*  
 325 *Change Biol* **19**, 45-63, doi:DOI 10.1111/j.1365-2486.2012.02797.x (2013).

326 10 Gent, P. R. *et al.* The Community Climate System Model Version 4. *Journal*  
 327 *of Climate* **24**, 4973-4991, doi:Doi 10.1175/2011jcli4083.1 (2011).

328 11 Dufresne, J. L. *et al.* Climate change projections using the IPSL-CM5 Earth  
 329 System Model: from CMIP3 to CMIP5. *Climate Dynamics* **40**, 2123-2165,  
 330 doi:DOI 10.1007/s00382-012-1636-1 (2013).

331 12 Watanabe, M. *et al.* Improved Climate Simulation by MIROC5. Mean States,  
 332 Variability, and Climate Sensitivity. *Journal of Climate* **23**, 6312-6335,  
 333 doi:Doi 10.1175/2010jcli3679.1 (2010).

334 13 Gordon, C. *et al.* The simulation of SST, sea ice extents and ocean heat  
 335 transports in a version of the Hadley Centre coupled model without flux  
 336 adjustments. *Climate Dynamics* **16**, 147-168 (2000).

337 14 Pope, V. D., Gallani, M. L., Rowntree, P. R. & Stratton, R. A. The impact of  
 338 new physical parametrizations in the Hadley Centre climate model: HadAM3.  
 339 *Climate Dynamics* **16**, 123-146 (2000).

340

341

